Fabrication and study Tb^{3+}:$MgAl_2O_4$ by combustion method using malonic acid dihydrazide as fuel

A. A. Ali*[1,2], M. R. Allazov[2], T. M. Ilyasli[2]

[1,2]*Chemistry department, faculty of science, Benha university, Egypt, Tel: (+994) 055-3486138, fax: (+994) 012-5614501

[2] inorganic department, chemistry faculty, Baku State University, Azerbaijan, Tel: (+994) 0505800748, fax: (+994) 012-5614501

[2] inorganic department, chemistry faculty, Baku State University, Azerbaijan, e-mail: Tel: (+994) 055-5983376, fax: (+994) 012-5109281

ABSTRACT

Nanoparticle doped Tb^{3+}:$MgAl_2O_4$ synthesized by combustion method at 300°C via ignited a stoichiometric mixture of aluminum nitrates, magnesium nitrates and Terbium nitrates with malonic acid dihydrazide as a fuel following by annealing at 800, 1000 and 1200°C. The obtained samples characterized by different tools as thermal analysis (TG-DTA), X-ray diffractions (XRD), UV–Vis spectroscopy, Transmission electron microscopy (TEM) and Infrared spectroscopy (IR). Particle sizes for 5%Tb^{3+}:$MgAl_2O_4$ with a size of 10-12.5 nm and for 10%Tb^{3+}:$MgAl_2O_4$ with a size of 10-12.5 nm were produced within the range of 800°C/2h - 1200°C/2h compared by the particle size of $MgAl_2O_4$ with a size of 10-12.5 nm in the same condition.

Key word: spinel structure; Infrared spectroscopy; Thermal analysis

Corresponding Author: Ayman A. Ali

1. INTRODUCTION

Inorganic materials synthesized by different methods from solution and the most common methods are solid-state reaction [1], micro-emulsion [2], co-precipitation [3], hydrothermal [4], sol–gel [5], Pechini [6] and low temperature combustion synthesis (LCS) [7-10]. Combustion synthesis or fire synthesis is also known as self-propagating high temperature synthesis and highly exothermic redox chemical reactions between an oxidizer (metal nitrates) and a fuel as Urea (U=+6, 10.57 KJ/g), carbohydrazide (CH=+8, 12.6 KJ/g), Glycine (G=+9, 13 KJ/g), Oxalic acid dihydrazide (ODH=+10, 11.5 KJ/g), Alanine (A=+15, 18.25 KJ/g), Malonic acid dihydrazide (MDH=+16, 15.1KJ/g), sucrose (S= +46, 16.6 KJ/g) [11-12] and other. The oxidizer/fuel molar ratio (O/F) required for a stoichiometric mixture (O/F =1) is determined by summing the total oxidizing and reducing valencies in the oxidizer compounds and dividing it by the sum of the total oxidizing and reducing valancies in the fuel compounds. The oxidizer/fuel molar ratio (O/F) =1 is considered the perfect ratio for combustion synthesis which produce amount of energy sufficient to prepare the corresponding oxides [13]. We were used combustion synthesis because of safe, simple, rapid fabrication process, and saves both time and energy. It can be used to prepare highly pure, homogeneous and crystalline with nano-particle sizes [14-15]. We were synthesized doped Tb^{3+}:$MgAl_2O_4$ spinel as result of important in different fields as

advanced ceramic, refractories, magnetic, semiconductors, dielectric, sensors, catalysts, phosphor, pigment and other application.

2. MATERIALS AND METHODS

2.1. MATERIALS

The starting chemicals used in this study are aluminum nitrates pentahydrate, $Al(NO_3)_3 \cdot 9H_2O$ (Aldrich), magnesium nitrates hexahydrate, $Mg(NO_3)_2 \cdot 6H_2O$ (Aldrich), Terbium oxides Tb_2O_3, nitric acid 65%, diethyl malonate 99.9% (Aldrich) and hydrazine hydrate (Aldrich).

2.2. SYNTHESIS OF MALONIC ACID DIHYDRAZIDE (MDH), $C_3H_8N_4O_2$

Malonic acid dihydrazide (MDH) is prepared by the chemical reaction of 1 mol of diethyl malonate with 2 mol of hydrazine hydrate. The chemical reaction is written as follows eq. (1):

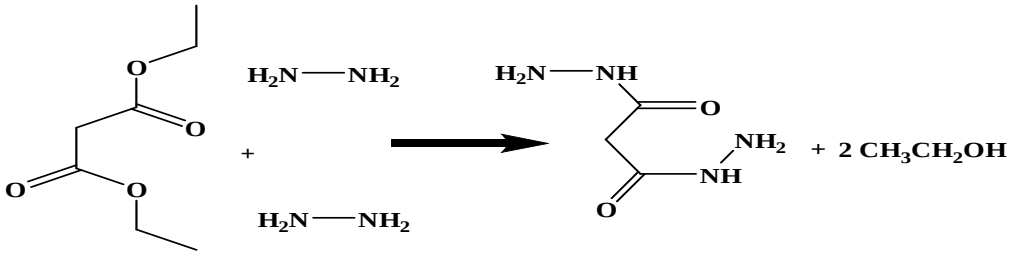

Malonic acid dihydrazide (MDH) is prepared by the chemical reaction of 1 mole of diethyl malonate with 2 mole of hydrazine hydrate. The chemical reaction is written as shown in equation 1. 25.04 g of hydrazine hydrate (0.5 mol.) is added dropwise to 40.05 g of diethyl malonate (0.25 mol.) dissolved in 350 ml of absolute ethanol. The mixture is refluxed for about 5 h. The clear solution obtained is cooled and then concentrated on a water bath. White crystals are obtained which are filtered and dried [13] (yield: 23.5 g, 70% and m.p. 152◦C).

2.3. PREPARATION OF Tb^{3+}:$MgAl_2O_4$ NANOMATERIALS

$MgAl_2O_4$ spinel powders were prepared by using combustion synthesis. Terbium oxides Tb_2O_3 dissolved in small amount of nitric acid at hotplate (60-70 for 5 min.). The calculated stoichiometric amounts of metal salts (aluminum nitrates, magnesium nitrates and Terbium nitrates) were mixed and dissolved in distilled water. The metals nitrates solutions were mixed with Malonic acid dihydrazide (MDH) as fuel according to equation 2 and 3. The resulting precursor was transferred into furnace that preheated to 250-300^oC, evaporated and spontaneously ignited exothermic reaction by burning of the metal nitrates and organic material with the release of gases. The combustion reaction completed within a few minutes, producing a precursor of oxides which was annealed at 800, 1000 and 1200^oC for 2h.

$$\mathbf{2(1\text{-}x)\ Mg(NO_3)_2 \cdot 6H_2O + + 4\ Al(NO_3)_3 \cdot 9H_2O + 5\ C_3H_8N_4O_2 \longrightarrow}$$

$$\mathbf{2MgAl_2O_4 + 68H_2O + 15CO_2 + 18N_2} \qquad \mathbf{(2)}$$

$$2(1\text{-}x)\ Mg(NO_3)_2 \cdot 6H_2O + + 4\ Al(NO_3)_3 \cdot 9H_2O + 5\ C_3H_8N_4O_2 \xrightarrow{2xTb(NO_3)_3}$$

$$2Tb_xMg_{1-x}Al_2O_4 + 68H_2O + 15CO_2 + 18N_2 \qquad (3)$$

Thermal analysis (TGA; Simultaneous TG-DTA/DSC Apparatus "STA 449 F3 Jupiter") of the precursor carried out at a heating rate of 10°C/min in static air. Phase formation of product identified by using X-ray diffraction (XRD; advanced D8) with Cu Kα radiation and the wavelength equal to (0.15406 nm). Transmission electron microscopy (TEM, modal: Tecnai G20, super twin, double tilte, at 200 kV and magnification up to 1000000 x). Infrared (IR) samples were carried out by using Jasco FT/IR-460 plus spectroscopy in 400–4000 range by employing potassium bromide KBr, pellet technique. Spectral analysis of materials carried out the instrument Perkin-Elmer spectrophotometer UV–Vis in 190 to 1100 nm.

3. RESULT AND DISCUSSION

3.1. THERMAL ANALYSIS

TG/DTA curves of $Tb_{0.1}Mg_{0.9}Al_2O_4$ ash shown in figure 1. TG curve shows three steps. The first step occurred in range 50-200ºC with 6.25 % of initial weight losses in TG curve due to elimination of the humidity and co-ordination water. The second step in range 200-600ºC losses 10 % and the third step in the range 600-900ºC losses 7.5 % in TG curve due to evolution of CO, CO_2 and NOx gases from sample as result of the decomposition the residual of organic material. We can say that phase formation starts around 750ºC from TGA curve. DTG shows three doublet endothermic peaks at 90-175, 340-390 and 760-820ºC. DTA shows two endothermic steps and one exothermic step. The first endothermic step at 60ºC occurred for elimination of the water in sample. The exothermic steps occurred at 400ºC for elimination and oxidation of the residual organic material in sample. The third endothermic reaction step at 740ºC shows phase formation and appearance of phase under study [16].

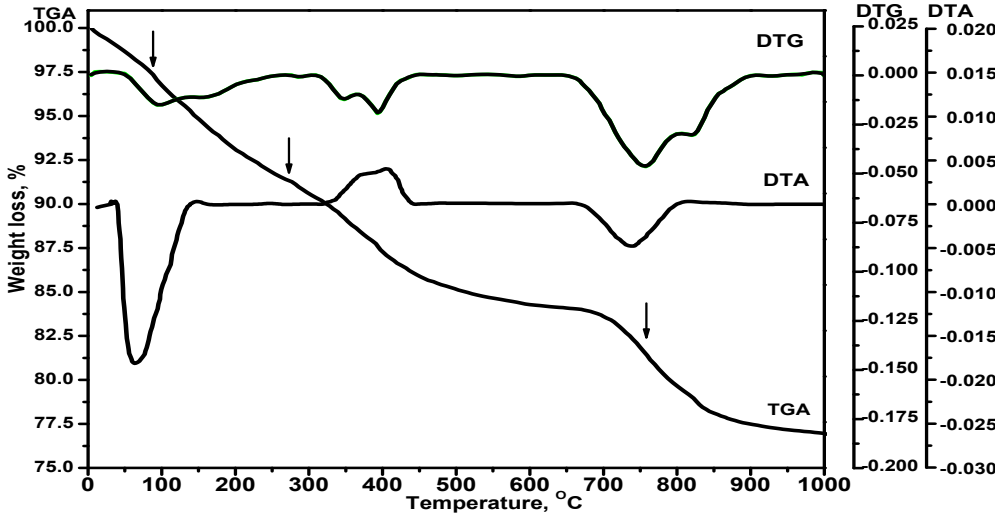

Fig 1. Thermal analysis (TG, DTG and DTA) for ash 10%Tb:$MgAl_2O_4$

3.2. INFRARED SPECTRA (FTIR)

In the 800–4000 cm^{-1} region of the IR spectrum, the absorption bands noted at around 3383-1639 cm^{-1} for $Tb_{0.1}Mg_{0.9}Al_2O_4$ and 3383-1639 cm^{-1} for $Tb_{0.05}Mg_{0.95}Al_2O_4$ at $1000^OC/2h$ can be attributed to the presence of absorbed water or surface hydroxyl groups and free or crystal water respectively. The intensity of the peak at 1385-1466 cm^{-1} may be derived from the vibration of NO_3 or NO_x which decreases gradually as increased annealing temperatures. In the 800–400 cm^{-1} region of the IR spectrum, the weakness of the two bands at 300^oC that they are low crystalline. The bands noted at around 683-486-413, 694-517 and 698-513 cm^{-1} correspond to the lattice vibration of AlO_6 and MgO_4 groups at 1000^oC for $Tb_{0.1}Mg_{0.9}Al_2O_4$, $Tb_{0.05}Mg_{0.95}Al_2O_4$ and $MgAl_2O_4$ respectively[14,17]. These build up the $MgAl_2O_4$ spinel and indicate the formation of $MgAl_2O_4$ spinel.

3.3. X-RAY DIFFRACTION

The X-ray diffractions for $Tb_{0.05}Mg_{0.95}Al_2O_4$, $Tb_{0.1}Mg_{0.9}Al_2O_4$ and $MgAl_2O_4$ are studied at different annealing temperatures as shown in Figure 2a, b and c, respectively. The peaks intensities of X-ray give only small crystallites after annealing at 700^oC which agree will with data of thermal analysis for the formation of the stable spinel phase at 750^oC. The intensities of peaks increase gradually with annealing until sharpen peaks are observed at 800, 1000 and 1200° C. Figure 2d shows the relation between the particle sizes of sample at different calcinations temperatures [8,10,14].

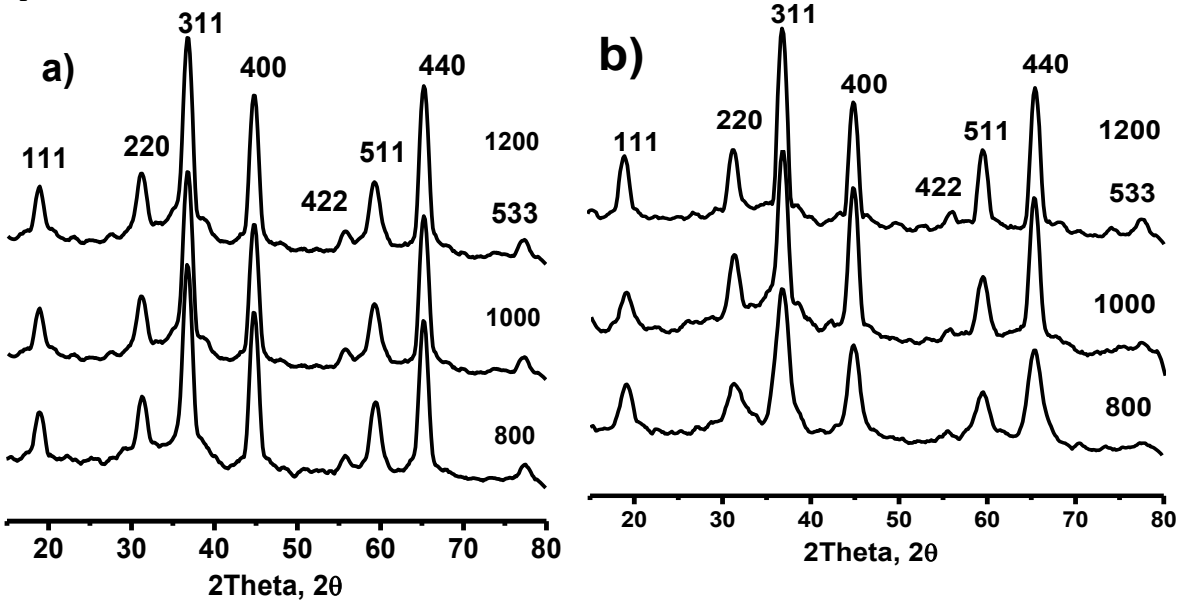

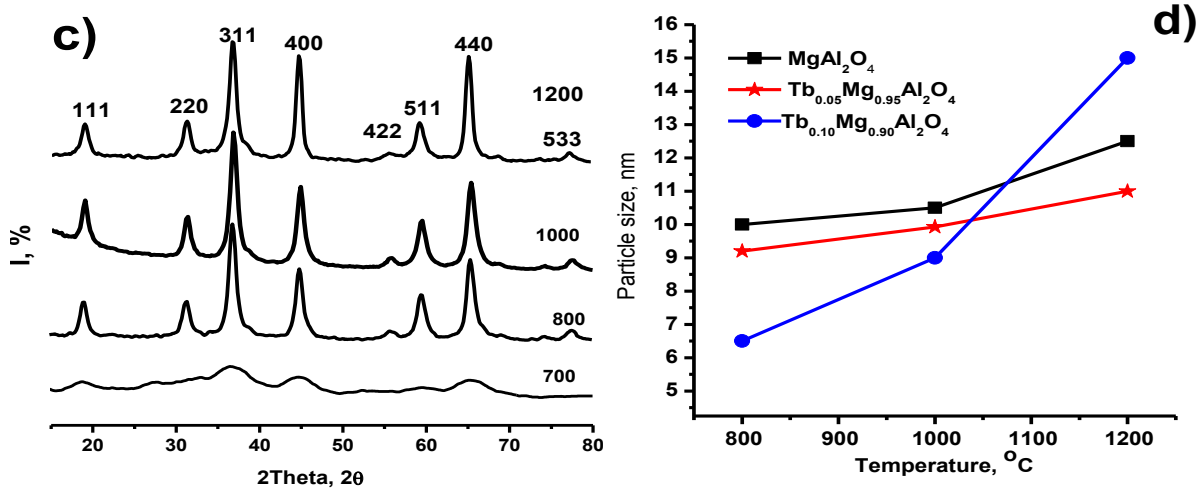

Fig. 2 (a, b, c and d). X-ray diffraction for a) $Tb_{0.05}Mg_{0.95}Al_2O_4$, b) $Tb_{0.1}Mg_{0.}$, c) $MgAl_2O_4$ at different temperatures and d) the relation between particle size and different temperatures for $MgAl_2O_4$, $Tb_{0.05}Mg_{0.95}Al_2O_4$ and $Tb_{0.1}Mg_{0.9}Al_2O_4$

The average crystallite size was calculated based on the XRD patterns using the peaks corresponding to the (h k l) planes and the scherrer equation 3:

$$\mathbf{D_{XRD} = (0.9\,\lambda)/(\beta cos\,\theta)} \qquad \mathbf{3}$$

Where D_{XRD} is the crystallite size (nm), λ is the radiation wavelength (0.15406 nm), β is the full width at half of the maximum (radians), θ is the Bragg angle (degrees). The lattice parameter was calculated using the equation 4:

$$\mathbf{a = d_{hkl}\sqrt{(h^2 + k^2 + l^2)}} \qquad \mathbf{4}$$

Where a is the lattice parameter, d is the interplanar distance, and h k l are the Miller indices (the same as used for D calculation). The X-ray density, $d_{X\text{-}ray}$ was calculated according to the following equation 5:

$$\mathbf{d_{x-ray} = 8M/Na^3} \qquad \mathbf{5}$$

Where M is the molecular weight, N is Avogadro's number and a is the lattice parameter. The crystalline particles size increase with increasing annealing temperatures**.** The particles sizes, densities, lattice parameter of different annealing temperatures from XRD data are given in Table 1.

Table 1. The particles sizes, densities, lattice parameter from XRD data

	phase		
parameter	$MgAl_2O_4$	$Tb_{0.05}Mg_{0.95}Al_2O_4$	$Tb_{0.1}Mg_{0.9}Al_2O_4$
		800/2h	
Particle size D, nm	10	9.2	6.5
Lattice constant a, A	8.05	8.064	8.044
Volume V, A^3	522	524.4	520.5
density, g/cm^3	3.62	3.88	4.15
		1000/2h	
Particle size D, nm	10.5	9.93	8
Lattice constant a, A	8.063	8.069	8.067
Volume V, A^3	524	525.4	524.97
density, g/cm^3	3.599	3.874	4.12
		1200/2h	
Particle size D, nm	12.5	11	15
Lattice constant a, A	8.082	8.078	8.070
Volume V, A^3	528	527.13	525.56
density, g/cm^3	3.57	3.861	4.11

3.4. TRANSMISSION ELECTRON MICROSCOPY, TEM

Figure **3** shows the TEM micrograph of the $Tb_{0.1}Mg_{0.9}Al_2O_4$ and $MgAl_2O_4$ samples annealed at 1000 °C with sheet and spherical shapes. The distribution of particle sizes for $Tb_{0.1}Mg_{0.9}Al_2O_4$ and $MgAl_2O_4$ are 7-14 nm and 8–14 nm in TEM micrograph, respectively. A mean average particle size calculated by averaging approximately thirty particles measurement is about 11 nm for $MgAl_2O_4$ and 10 nm for $Tb_{0.1}Mg_{0.9}Al_2O_4$. The particle sizes are determined using TEM and are compared with that obtained from XRD and collective data. These sizes agree with XRD data, indicating that the particles observed by TEM are primary particles [8, 10].

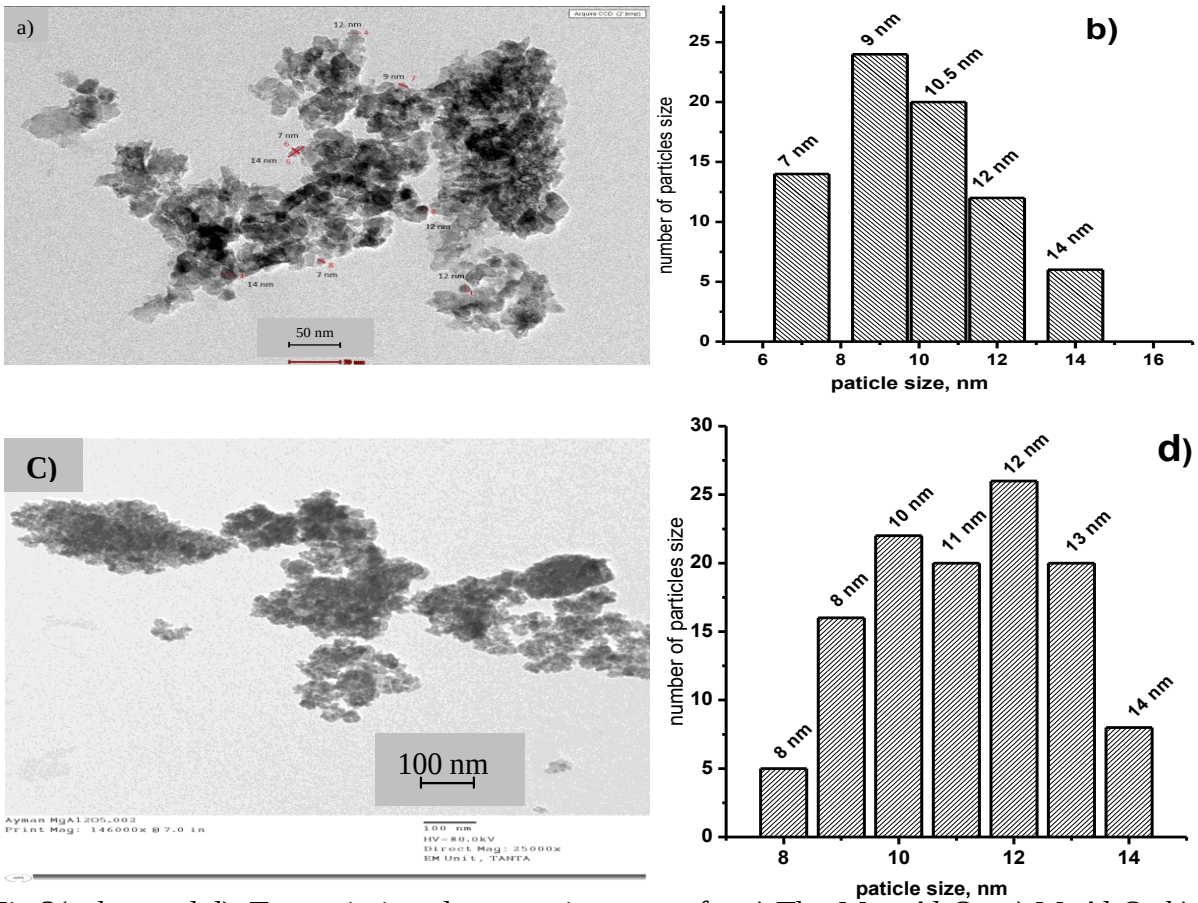

Fig 3(a, b, c and d). Transmission electron microscopy for a) $Tb_{0.1}Mg_{0.9}Al_2O_4$, c) $MgAl_2O_4$, b) and d) the relation between particles size and number of particles size for $Tb_{0.1}Mg_{0.9}Al_2O_4$ and $MgAl_2O_4$ in TEM micrograph annealed at 1000°C.

3.5. UV–Visible spectra

UV–Visible spectra of $MgAl_2O_4$, $Tb_{0.05}Mg_{0.95}Al_2O_4$ and $Tb_{0.1}Mg_{0.9}Al_2O_4$ samples annealing at different calcination temperatures, are presented in Fig. 4. All the samples show UV-Visible light absorption abilities. The edges of bands were shifted to higher wavelength as result of increasing of amount Tb^{3+} in the lattice of $MgAl_2O_4$ and calcinations temperatures. $MgAl_2O_4$ has band energies from 3.76 eV at 800°C to 2.95 eV at 1200°C, $Tb_{0.05}Mg_{0.95}Al_2O_4$ has band energies from 3.1 eV at 800°C to 2.7 eV at 1200°C and $Tb_{0.1}Mg_{0.9}Al_2O_4$ has band energies from 3.18 eV at 800°C to 2.53 eV at 1200°C.By other words, this means that the band energy shift to lower value as result of the increasing the percentage of Tb^{3+}. Visible light absorption may result from the observed absorption is caused by the $O^{2-} \rightarrow Al^{3+}$ charge transition corresponding to the excitation of electrons from VB of O2p to CB. The red shift observed in the UV-Visble spectra of nano-ceramic $MgAl_2O_4$ may be leaded to the optical absorption of various color centers induced by oxygen vacancies [18-19]. The energy gap decreased for $MgAl_2O_4$ that due to the formation of high crystalline structure as result of the annealing samples at different temperatures.

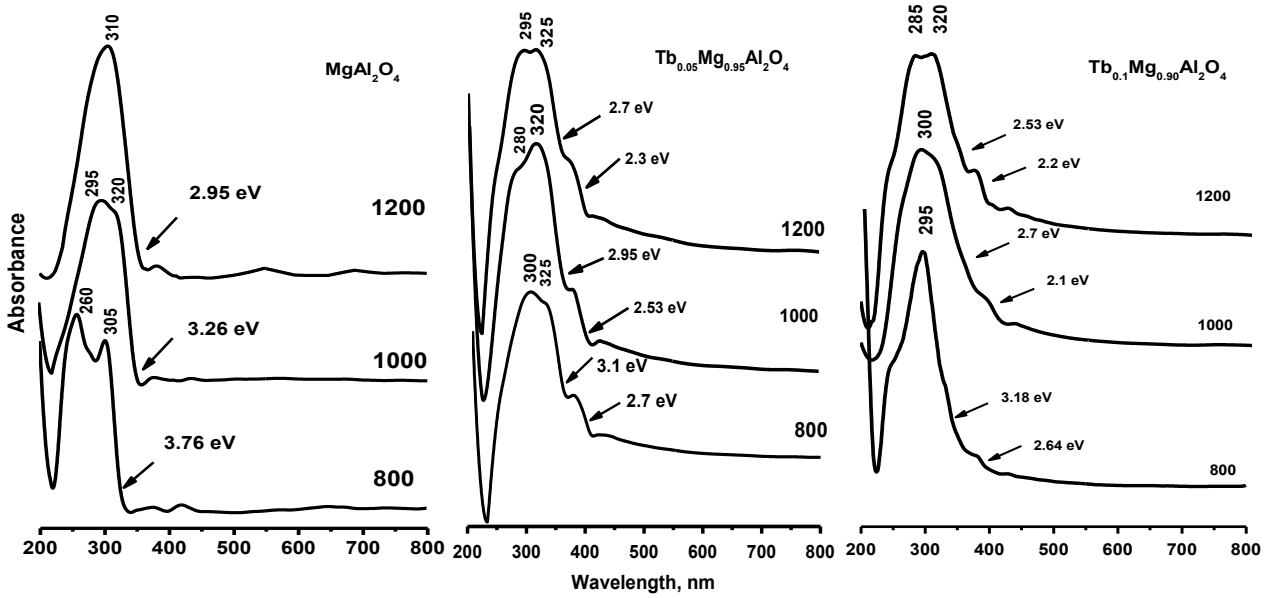

Fig 4. UV–Visible spectra of $MgAl_2O_4$, $Tb_{0.05}Mg_{0.95}Al_2O_4$ and $Tb_{0.1}Mg_{0.9}Al_2O_4$ samples at different calcinations temperatures.

CONCLUSION

Tb^{3+}:$MgAl_2O_4$ nanoparticle papered by combustion method at 300°C following by annealing at different calcinations temperatures. Thermal analysis gives us that the crystalline phases of $MgAl_2O_4$ and doping materials are formed after annealing at 800°C which agree with X-ray diffraction. TEM micrograph shows sheet and spherical shapes for $Tb_{0.1}Mg_{0.9}Al_2O_4$ and $MgAl_2O_4$ samples that annealing at 1000°C. Average particle size calculated from TEM micrograph about 11 nm for $MgAl_2O_4$ and 10 nm for $Tb_{0.1}Mg_{0.9}Al_2O_4$. Infrared spectroscopy shows bands at 683-486-413, 694-517 and 698-513 cm^{-1} correspond to the lattice vibration of AlO_6 and MgO_4 groups at 1000°C for $Tb_{0.1}Mg_{0.9}Al_2O_4$, $Tb_{0.05}Mg_{0.95}Al_2O_4$ and $MgAl_2O_4$ respectively. These build up the $MgAl_2O_4$ spinel and indicate the formation of $MgAl_2O_4$ spinel. The edges of bands were shifted to higher wavelength and band energies shifted to lower values as result of increasing of amount Tb^{3+} in the lattice of $MgAl_2O_4$ and calcinations temperatures.

REFERENCE

1. I. Ganesh, G. J. Reddy, G. Sundararajan, S. M. Olhero, P. M. C. Torres and J. M. F. Ferreira, Influence of processing route on microstructure and mechanical properties of $MgAl_2O_4$ spinel, Ceramics International, Vol.36, pp. 473–482, 2010.

2. J. Chandradass, M. Balasubramanian, D. S. Bae, J. Kim and K. H. Kim, effect of water to surfactant ratio (R) on the particle size of $MgAl_2O_4$ nanoparticle prepared via reverse micelle process, Journal of Alloys and Compounds, Vol. 491, pp. L25–L28, 2010.
3. M.F. Zawrah, H. Hamaad and S. Meky, Synthesis and characterization of nano $MgAl_2O_4$ spinel by the co-precipitated method, Ceramics International, Vol. 33, pp.969–978, 2007.
4. X. Zhang, hydrothermal synthesis and catalytic performance of high-surface-area mesoporous nanocrystallite $MgAl_2O_4$ as catalyst support, Materials Chemistry and Physics, vol. 116, pp. 415–420, 2009.
5. A. Saberi, F. Golestani-Fard, M. Willert-Porada, Z. Negahdari, C. Liebscher and B. Gossler, a novel approach to synthesis of nanosize $MgAl_2O_4$ spinel powder through sol–gel citrate technique and subsequent heat treatment, Ceramics International, vol. 35, pp. 933–937, 2009.
6. H. Zhang, X. Jia, Z. Liu and Z. Li, The low temperature preparation of nanocrystalline $MgAl_2O_4$ spinel by citrate sol–gel process, Materials Letters, vol. 58, pp. 1625– 1628, 2004.
7. S. T. Aruna and A. S. Mukasyan, combustion synthesis and nanomaterials, Current Opinion in Solid State and Materials Science, vol. 12, pp. 44–50, 2008.
8. K. Prabhakaran, D.S. Patil, R. Dayal, N.M. Gokhale and S.C. Sharma, Synthesis of nanocrystalline magnesium aluminate ($MgAl_2O_4$) spinel powder by the urea–formaldehyde polymer gel combustion route, Materials Research Bulletin, vol. 44, pp. 613–618, 2009.
9. J. Bai, J. Liu, C. Li, G. Li and Q. Du, mixture of fuels approach for solution combustion synthesis of nanoscale $MgAl_2O_4$ powders, Advanced Powder Technology, vol. 22, pp. 72–76, 2011.
10. B. Alinejad, H. Sarpoolaky, A. Beitollahi, A. Saberi and S. Afshar, synthesis and characterization of nanocrystalline $MgAl_2O_4$ spinel via sucrose process, Materials Research Bulletin, vol. 43, pp. 1188–1194, 2008.
11. J. D. Cox, G. Pilcher, thermochemistry of organic and organometallic compounds, Academic Press, New York, 1970, pp.1-636.
12. G.M. Kibler, H. Hunt, Heats of combustion.V. The heats of combustion of five nitrogen-containing compounds, Journal Physical Chemistry, v.53, pp. 955-956, 1949.
13. K.C. Patil, M.S. Hegde, T. Rattan, S.T. Aruna, chemistry of combustion synthesis, properties and applications: nanocrystalline oxide materials, World Scientific Publishing Co. Pte. Ltd., London, 2008, pp. 1-362.
14. A. Saberi, F. Golestani-Fard, H. Sarpoolaky, M. Willert-Porada, T. Gerdes and R. Simon, chemical synthesis of nanocrystalline magnesium aluminate spinel via nitrate–citrate combustion route, Journal of Alloys and Compounds, vol. 462 pp.142–146, 2008.
15. S. Kakooei, J. Rouhi, E. Mohammadpour, M. Alimanesh and A. Dehzangi synthesis and characterization of Cr-Doped Al_2O_3 nanoparticles prepared via aqueous combustion method, Caspian Journal of Applied Sciences Research, vol. 1(13), pp.16-22, 2012.
16. R. Ianos, I. Lazau, C. Pacurariu and P. Barvinschi, Solution combustion synthesis of $MgAl_2O_4$ using fuel mixtures, Materials Research Bulletin, vol. 43, pp.3408–3415, 2008.
17. E. N. Alvar, M. Rezaei and H. N. Alvar, Synthesis of mesoporous nanocrystalline $MgAl_2O_4$ spinel via surfactant assisted precipitation route, Powder Technology, vol. 198, pp. 275–278, 2010.

18. F. Li, Y. Zhaoa, Y. Liua, Y. Haoa, R. Liua, D. Zhaob, solution combustion synthesis and visible light-induced photocatalytic activity of mixed amorphous and crystalline $MgAl_2O_4$ nanopowders. Chemical Engineering Journal, vol.173, pp. 750– 759, 2011.
19. S. Jiang, T. Lua, J. Zhanga, J. Chen, first-principles study on the effects of point vacancies on the spectral properties of $MgAl_2O_4$, Solid State Communications, vol. 151, pp. 29–32, 2011.